
Article:
Porter, C.P., Edge, R. and Ogden, M.D. (2017) Polymeric seal degradation in nuclear power plants: Effect of gamma radiation on sealing properties. Journal of Applied Polymer Science, 134 (12). ISSN 0021-8995

https://doi.org/10.1002/app.44618

Polymeric Seal Degradation in Nuclear Power Plants: Effect of Gamma Radiation on Sealing Properties

Christopher P. Porter[a1], Ruth Edge[b] and Mark D. Ogden[a]

[a]Department of Chemical and Biological Engineering, University of Sheffield, Portobello Street, Sheffield, S1 3JD.

[b]Dalton Cumbrian Facility, University of Manchester, Westlakes Science & Technology Park, Moor Row, Cumbria, CA24 3HA

Main Author Correspondence: *m.d.ogden@sheffield.ac.uk*

ABSTRACT

An effort has been made to bridge the gap between academic knowledge of polymeric seal degradation and industrial practices. A series of physical and mechanical properties that can be related to the sealing behaviour of three commercial samples of nitrile rubber have been studied for their degradation when exposed to gamma radiation. For all samples the glass transition temperature, T_g, and Retention Factor, RF, were found to increase with total dose whilst Percentage Change in Mass, $\Delta_{M\%}$, was found to decrease. The ultimate uptake of carbon dioxide, CO_2, did not appear to change with radiation dose but the kinetics of the absorption process were found to decrease, suggesting the formation of crosslinks. The crosslinks formed appear to be dependent on the original material composition and comparison against degradation of material properties supports the theory behind butadiene, BDN, content being linked to a propensity for crosslink clustering.

---

[1] Current Address: R S Bruce Metals and Machinery Ltd, March Street, Sheffield, S9 5DQ

INTRODUCTION

Nitrile rubber (NBR), a co-polymer blend of butadiene (BDN) and acrylonitrile (ACN), is a commercially important material and forms the basis for many elastomeric seals. The polarity of the C≡N bond in the ACN monomer gives NBR its good oil and grease resistivity [1] and thus explains its use as a dynamic seal. When considering the sealing capacity of such a component the ability for the material to create a sealing force when compressed is of paramount importance. Exposure to detrimental operational conditions will affect the materials microstructure and hinder the components ability to create an effective seal boundary. These operational conditions will be specific to the components use and, for the purposes of this investigation, have been found to be gamma-radiation, γ, exposure, cyclic pressurised conditions and reciprocal movement. This combination of operational conditions leads to unique, and often complicated, degradation mechanisms that simple extrapolation of Arrhenius plots have been unable to predict [2-8] and thus a breakdown into individual processes and synergistic effects is required [9-10].

The literature [11-17] describes the process of γ-radiation attack on NBR as follows:

1. High-energy incident radiation results in ionisation of either BDN or ACN pendants
2. This results in the loss of hydrogen atoms which recombine with the surrounding cage of neighbouring chains and produce radicals
3. The recombination of these radicals then follow three possible pathways in usual scenarios:

a. The hydrogen atoms remove other hydrogen atoms and the two radicals can bind to form stable species in the allylic position – resulting in scission of the weaker chemical bonds (C-H)
b. Due to the presence of the cyanide bond, the hydrogen atoms may also lead to the formation of conjugated polyimine radicals
c. In the presence of oxygen and with lower quantities of ACN C-O-C crosslinks may be formed

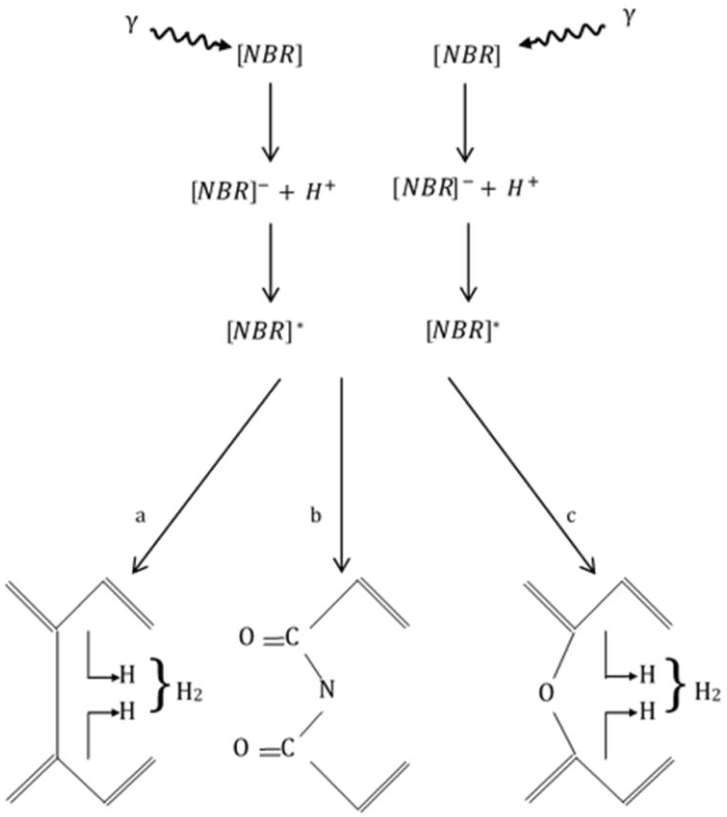

FIGURE 1: The Ionisation of NBR Following Gamma Radiation and the Subsequent Degradation Mechanisms.

This crosslinking mechanism is often utilised in elastomer manufacture and is referred to as vulcanisation, whereby a radiation-sensitive component would be added to reduce the required dose of irradiation [12]. However, continued

exposure to high-energy radiation, such as that experienced in Nuclear Power Plants, NPPs, can begin to have a detrimental effect on the material properties. In a series of similar experiments *Davenas et al.* [11] and *Vijayabaskar, Tikku and Bhowmick* [12] witnessed increasing gel content of their samples up to a dose of 100 kGy and an increase in tensile strength up to a maximum at 50 kGy. However, T_g was found to continually increase with no evidence of tailing off. They explained this through the development of a 3D network in the form of crosslinking, as expected, until the crosslink density increases to a threshold value at which point the network becomes so dense that there is little energy dissipation and significant segments of the polymer chains become immobile. However, there is little literature available comparing the effects of gamma radiation attack on T_g, mechanical response, swelling behaviour and the kinetics and thermodynamics of CO_2 uptake, all of which will have an impact on the ability of the material to create a seal. The variety of additives and inclusions that may be used in the manufacturing process also means that each NBR sample may differ significantly from one to the next and so a baseline point of reference needs to be taken.

Porter and Ogden [18] characterised a set of NBR samples through determination of their T_g and mechanical Retention Factor, RF, and compared these against Percentage Volume Increase, $\Delta_{V\%}$, and CO_2 absorption behaviour to infer microstructural characteristics that can be linked to the materials ability to create a seal boundary. This paper discusses the development of these sealing capacity characteristics following radiation exposure under standard atmospheric conditions. The results are then cross-analysed between all

samples to determine the effect of radiation on the material properties and each samples' susceptibility to radiation-induced damage.

EXPERIMENTAL

Materials

Three NBR samples have been obtained from Whitby and Chandler Ltd. at hardness grades BA40, BA50 and BA60. NBR is an elastomer constructed from acrylonitrile, ACN, and butadiene, BDN, monomers, the ratio of which determines the material's physical properties. The precise composition of these materials is proprietary knowledge and can therefore not be reproduced here.

Radiation Exposure

Each sample was cut using a rotary drill into approximately 55 mm diameter discs and placed on a turntable in a cobalt-60 irradiator at the Dalton Cumbrian Facility, DCF, and exposed to a dose rate of 1.67 Gy s^{-1} for previously set periods of time. The samples were held at atmospheric pressure and the only source of heat was that emitted by the Co^{60} source. This ensured total received doses of 10, 50, 100, 250 and 500 kGy of gamma radiation and an even dose spread throughout each sample. Following this radiolysis all samples were allowed to cool and then were assessed for their change in the following material properties at each radiation dose.

Infra-red Spectroscopy

Approximately 4 mm was removed from the surface of the samples before Fourier Transform IR Spectroscopy was carried out on a Perkin Elmer Frontier FTIR with a diamond Attenuated Total Reflectance, ATR, attachment. This attachment clamped the material into place and ensured maximum contact between the sample and the diamond surface. The spectroscopic analysis was

run at wavelengths between 4000 and 500 cm^{-1} at a resolution of 4 scans cm^{-1} and an accumulation of 4 scans.

Glass Transition Temperature

4-5 mg of sample was cut into as small as is reasonably practicable monoliths and placed in a Perkin Elmer Diamond Differential Scanning Calorimeter to identify T_g at 63 % between base line transitions on a temperature range of -60 to 20 °C at a ramp rate of 10 °C min^{-1}.

Mechanical Behaviour

A Lloyds Texture Analyser 500 was used to compress 7 mm diameter pellets of samples through a compression-relaxation programme at a movement rate of 1 mm min^{-1} carried out at 1, 2, 3, 4 and 5 mm set deflections. Similar to calculation of the energy dissipated through visco-elastic deformation [19] the trapezoidal rule, Equation 1, was used to calculate the integral of the compression and relaxation curves, the ratio of which was identified as the Retention Factor, RF, and used to determine the energy retention potential of the elastomeric microstructure.

$$\text{Integral area} = \int_a^b f(x)dx \approx (b-a)\left[\frac{f(a)+f(b)}{2}\right] \quad (1)$$

where a and b are two locations on the x axis.

Absorption Behaviour

Toluene

The procedure set out in ASTM D6814 calculates the crosslink density of crumb rubber. Without knowing the polymer-solvent interaction parameter this calculation is not possible and so the procedure has been adapted in the following manner.

The samples were cut using a sharp fresh blade on a Stanley Knife into approximately 6 mm^3 cubes and placed in approximately four sample-volumes of reagent grade toluene and allowed to come to equilibrium over a period of 72 hours, changing the solvent for new every 24 hours. An AnD GR-202 micro balance with a repeatability of 0.01 mg was used in conjunction with Equation 2 to calculate Percentage Increase in Mass, $\Delta_{M\%}$, and a caliper with a repeatability of 0.01 mm was used in conjunction with Equation 3 to calculate percentage increase in volume.

$$\Delta_{M\%} = \frac{M_t - M_0}{M_0} x100 \quad (2)$$

$$\Delta_{V\%} = \frac{L_t W_t T_t - L_0 W_0 T_0}{L_0 W_0 T_0} x100 \quad (3)$$

where M denotes the mass of the sample in g, L, W and T denote the length, width and thickness of the sample in mm and the subscripts 0 and t denote the recordings before and after immersion respectively.

CO_2

50-100 mg of sample was dissected into approximately 1 mm^3 monoliths and placed into a Hiden Isochema Intelligent Gravimetric Analyser 002. The samples were taken down to vacuum to remove any previously absorbed gases and then underwent 1 bar pressure increments between 1 and 10 bar with CO_2 under isothermal conditions. During equilibration the increase in mass was recorded and the kinetic data was fitted to the pseudo-first, PFO, and pseudo-second order, PSO, rate equations [20] shown in Table 1. The thermodynamic data was then fitted against the Freundlich, F [21], Langmuir, L [22], Temkin, T [23], and Dubinin-Radushkevic, DR [24], isothermal models. The five-error analysis as set

out by *Ho, Porter and McKay* [25] was used to identify the Sum of the Normalised Error, SNE, values and find the rate equations and isothermal models that best fit the experimental data.

Table 1: Kinetic Rate Equations and Isothermal Models.

Model	Equation	
PFO	$q_t = q_e\left(1 - e^{-k_1 t}\right)$	(1)
PSO	$q_t = \frac{k_2 q_e^{\,2} t}{1 + k_2 q_e t}$	(2)
F	$q_e = a_F C_e^{\,1/n_F}$	(3)
L	$q_e = \frac{q_m a_L C_e}{1 + a_L C_e}$	(4)
T	$q_e = \frac{RT}{b_T} \ln\left(a_T C_e\right)$	(5)
DR	$q_e = q_D \exp\left\{ - B_D \left[RT \ln\left(1 + \frac{1}{C_e} \right) \right]^2 \right\}$	(6)

where q is the uptake of CO_2 into the elastomer in kg kg^{-1} and the subscripts t, e and m are the recordings at time t, at equilibrium and at monolayer saturation capacity respectively, k_1 is the PFO observed rate constant in s^{-1}, t is the time in s, k_2 is the PSO observed rate constant in kg kg^{-1} s^{-1}, C_e is the concentration of CO_2 in the environment in kg m^{-3}, a_F is the dimensionless Freundlich Isotherm Constant, n_F is the dimensionless Strength of Interaction Parameter, a_L is the dimensionless Langmuir Isotherm Constant, R is the Universal Gas Constant in kJ mol^{-1} K^{-1}, T is the temperature in K, a_T and b_T are the two dimensionless Temkin Isotherm Constants and q_D and B_D are the two dimensionless Dubinin-Radushkevic Isotherm Constants.

RESULTS

Infra-red Spectroscopy

In BA40 the peak heights attributed to $R_1HC=CH_2$ vinylidene and >C=C< cis groups at 918 and 741 cm^{-1} respectively both showed a similar decrease up to 50 kGy before they increased to a steady value for higher doses, Figure 2. The >C=C< trans group at 964 cm^{-1} increased up to 10 kGy before it steadily decreased and the C≡N nitrile group at 2235 cm^{-1} showed a steady decrease across all doses. BA50 showed a general decrease across all bonds with a slightly larger decrease in the $R_1HC=CH_2$ vinylidene and >C=C< cis groups, Figure 3. BA60 showed more erratic behaviour but a generally small increase in all respective peak heights was seen, Figure 4.

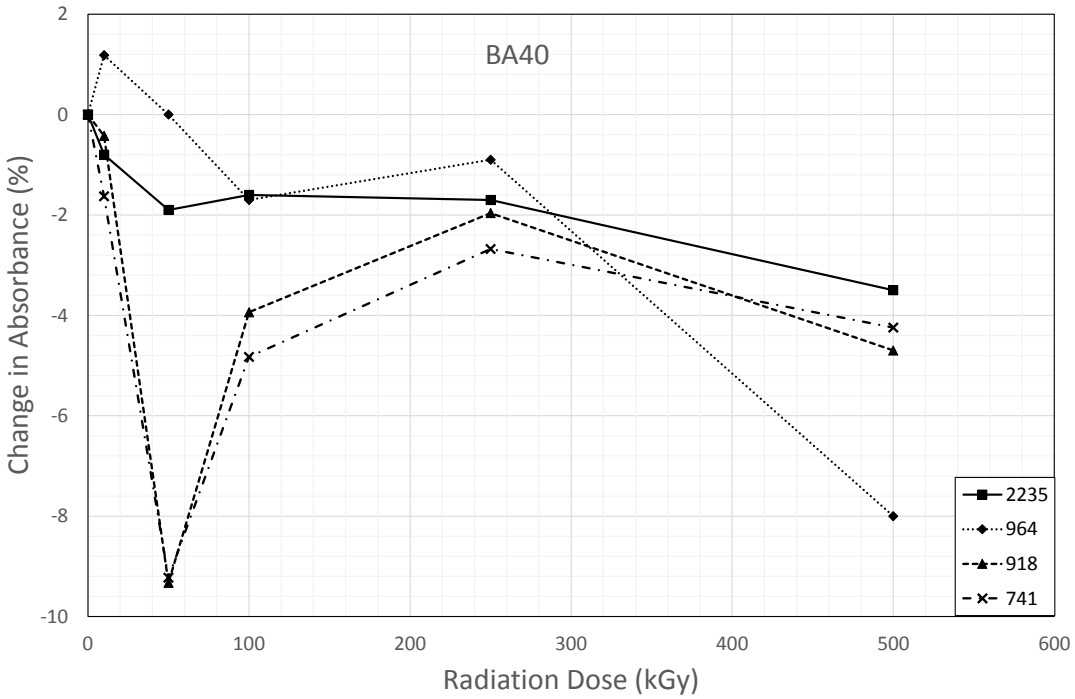

FIGURE 2: Changes in IR Absorbance at 2235, 964, 918 and 741 cm^{-1} Wavelengths in BA40 NBR up to 500 kGy of Gamma Radiation under Standard Atmospheric Conditions.

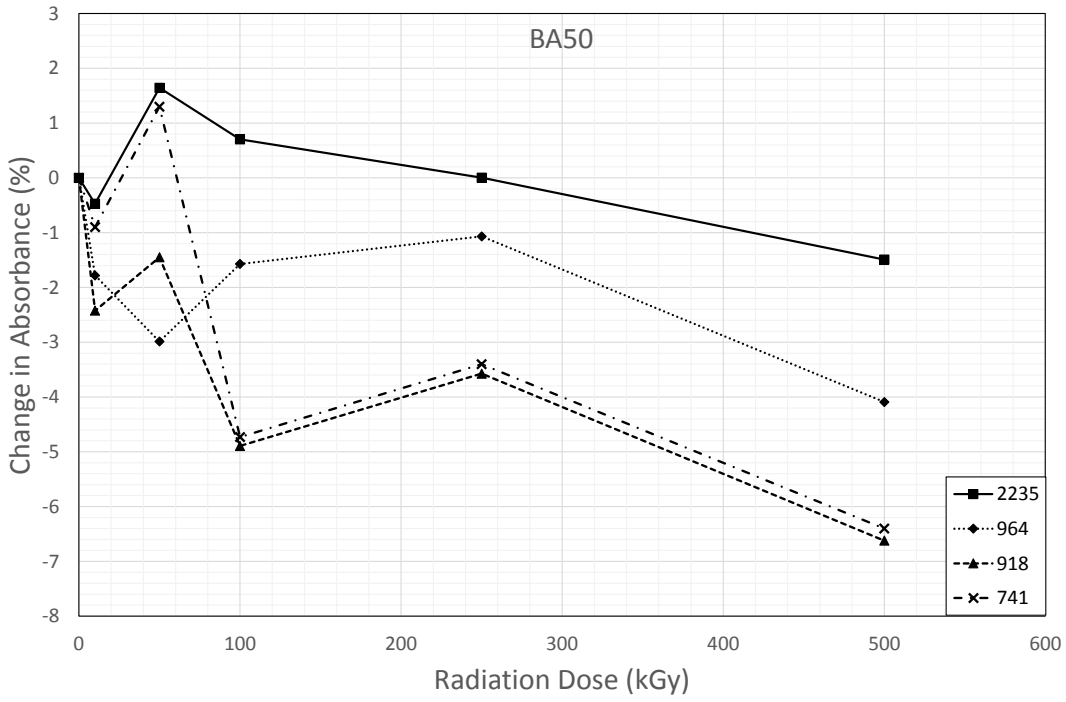

FIGURE 3: Changes in IR Absorbance at 2235, 964, 918 and 741 cm^{-1} Wavelengths in BA50 NBR up to 500 kGy of Gamma Radiation under Standard Atmospheric Conditions.

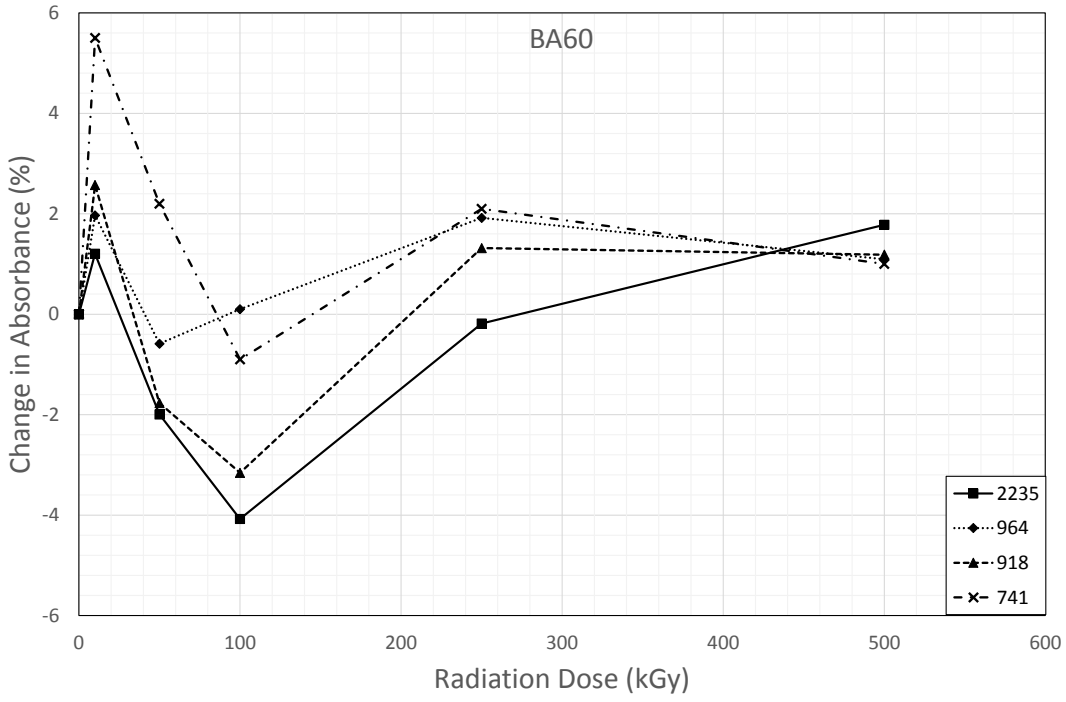

FIGURE 4: Changes in IR Absorbance at 2235, 964, 918 and 741 cm^{-1} Wavelengths in BA60 NBR up to 500 kGy of Gamma Radiation under Standard Atmospheric Conditions.

Material Properties

T_g and RF increased with irradiation for all samples, Table 2. In BA40 T_g increased more than RF, Figure 5, in BA50 they increased at approximately the same rate, Figure 6, and in BA60 T_g increased less than RF, Figure 7.

TABLE 2: T_g and RF Following Exposure to 10, 50, 100, 250 and 500 kGy Gamma Radiation under Standard Atmospheric Conditions.

T_g			
Radiation Dose (kGy)	BA40	BA50	BA60
0	-25.3 ± 0.4	-27.8 ± 0.4	-28.2 ± 0.4
10	-24.6 ± 0.3	-28.9 ± 0.4	-29.5 ± 0.4
50	-24.1 ± 0.3	-27.5 ± 0.4	-28.9 ± 0.4
100	-23.8 ± 0.3	-27.8 ± 0.4	-28.4 ± 0.4
250	-22.0 ± 0.3	-26.3 ± 0.4	-26.7 ± 0.4
500	-21.0 ± 0.3	-23.8 ± 0.4	-25.8 ± 0.4
RF			
Radiation Dose (kGy)	BA40	BA50	BA60
0	0.83 ± 0.02	0.71 ± 0.01	0.52 ± 0.01
10	0.82 ± 0.02	0.70 ± 0.01	0.51 ± 0.01
50	0.84 ± 0.02	0.71 ± 0.01	0.53 ± 0.01
100	0.86 ± 0.02	0.72 ± 0.01	0.54 ± 0.01
250	0.87 ± 0.02	0.74 ± 0.02	0.58 ± 0.01
500	0.88 ± 0.02	0.78 ± 0.02	0.61 ± 0.01

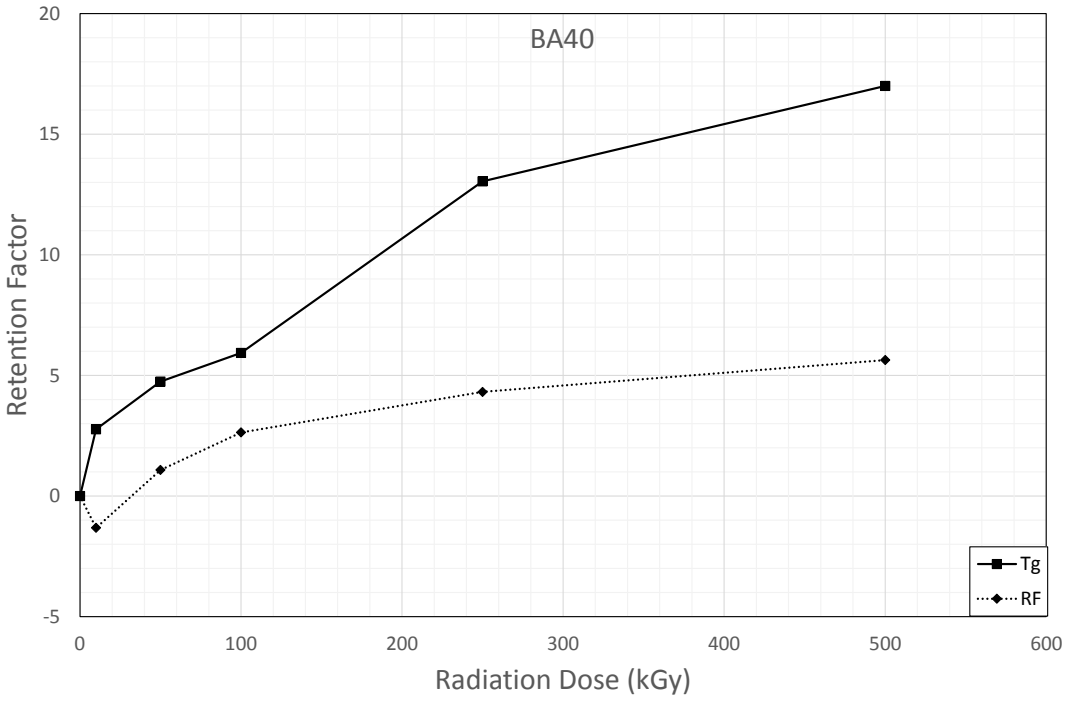

FIGURE 5: BA40 Percentage Change in T_g and RF Following Exposure to 10, 50, 100, 250 and 500 kGy Gamma Radiation under Standard Atmospheric Conditions.

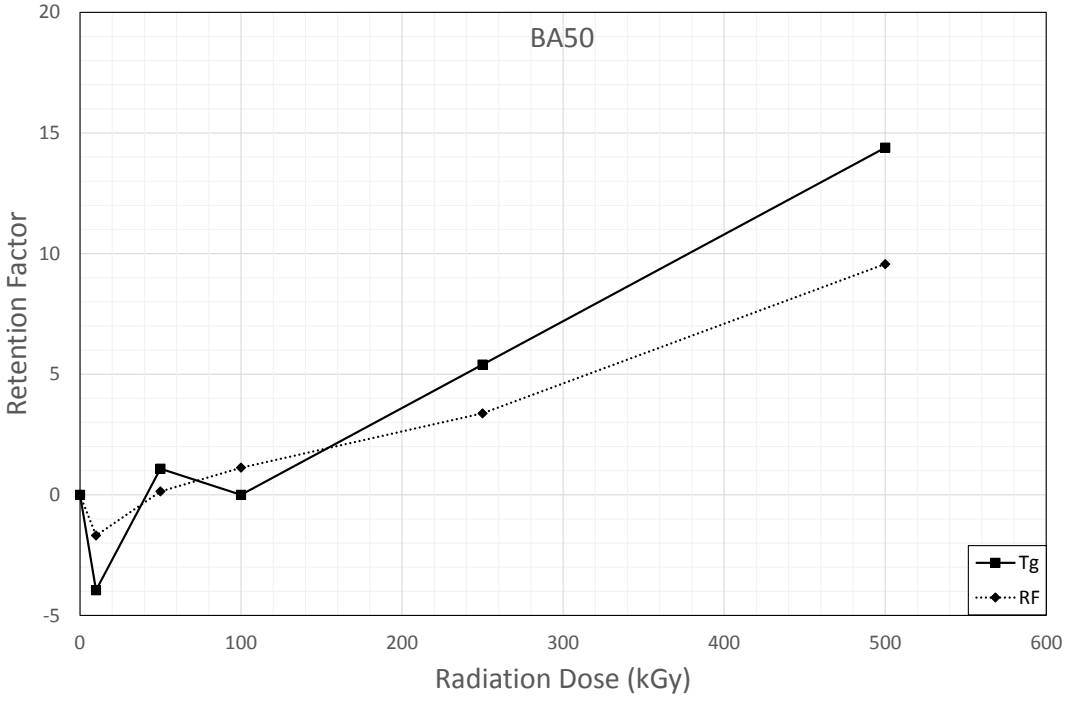

FIGURE 6: BA50 Percentage Change in T_g and RF Following Exposure to 10, 50, 100, 250 and 500 kGy Gamma Radiation under Standard Atmospheric Conditions.

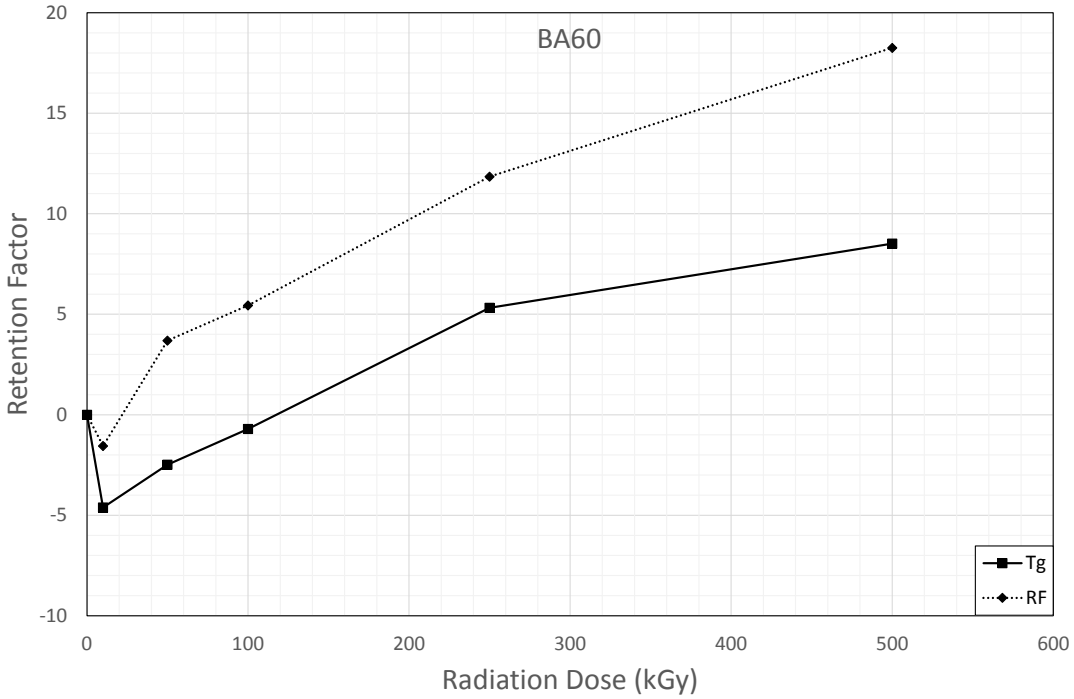

FIGURE 7: BA60 Percentage Change in T_g and RF Following Exposure to 10, 50, 100, 250 and 500 kGy Gamma Radiation under Standard Atmospheric Conditions.

Absorption Behaviour

Toluene

$\Delta_{M\%}$ showed a general decrease with irradiation dose for all samples, Table 3. BA40 and BA60 decreased at the same rate whilst BA50 showed a decreased effect from gamma radiation, Figure 8.

TABLE 3: $\Delta_{M\%}$ Following Exposure to 10, 50, 100, 250 and 500 kGy Gamma Radiation under Standard Atmospheric Conditions.

$\Delta_{M\%}$			
Radiation Dose (kGy)	BA40	BA50	BA60
0	89 ± 3	135 ± 5	108 ± 4
10	87 ± 3	135 ± 5	106 ± 4
50	87 ± 3	130 ± 5	99 ± 4
100	78 ± 3	128 ± 5	97 ± 4
250	77 ± 3	124 ± 5	91 ± 3
500	68 ± 3	110 ± 4	82 ± 3

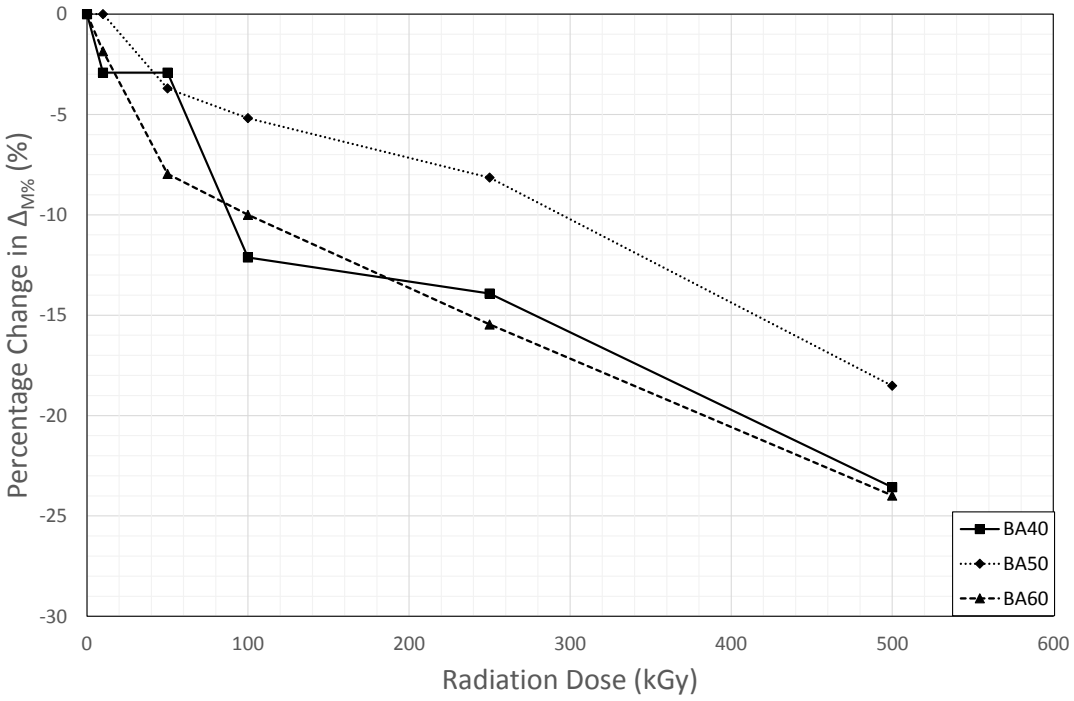

FIGURE 8: Percentage Change in $\Delta_{M\%}$ for All Three Samples Following Exposure to 10, 50, 100, 250 and 500 kGy Gamma Radiation under Standard Atmospheric Conditions.

CO_2

Kinetics

k_2 showed a marked decrease against C_e following irradiation for all samples, with decreasing intensity in increasing hardness, Figure 9.

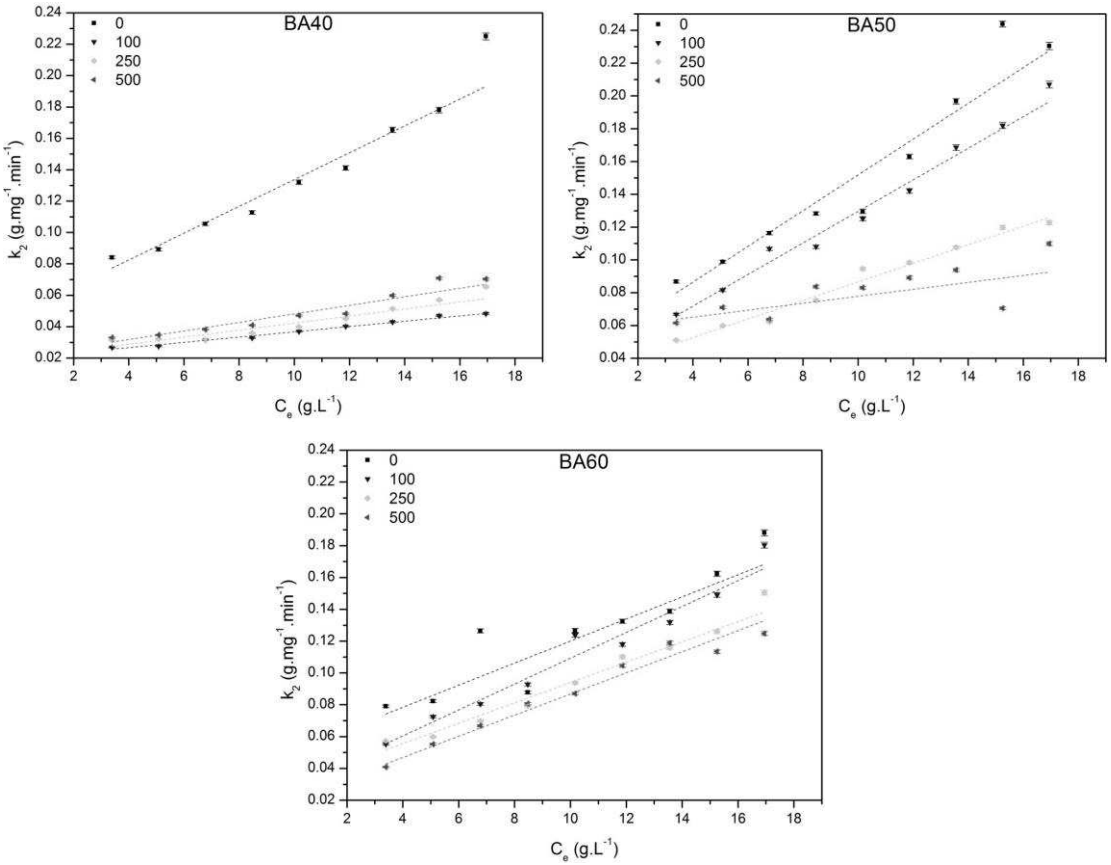

FIGURE 9: The Plots of k_2 against C_e for All Three Samples Following Exposure to 100, 250 and 500 kGy Gamma Radiation under Standard Atmospheric Conditions.

Thermodynamics

For BA40 and BA60 the equilibrated mass of CO_2 absorbed into the elastomer at 10 bar pressure, $q_{e,}10$, showed an initial increase with radiation dose up to 100 kGy before a slight decrease, Table 4. However, for BA50 a far reduced increase was first seen before a much larger decrease, taking $q_{e,10}$ below its original value.

The percentage change plots reveal the similarity between the changes in BA40 and BA60, Figure 10.

TABLE 4: $q_{e,10}$ for All Three Samples Following Exposure to 100, 250 and 500 kGy Gamma Radiation under Standard Atmospheric Conditions.

$q_{e,10}$ ($mg.g^{-1}$)			
Radiation Dose (kGy)	BA40	BA50	BA60
0	20.024 ± 0.006	20.140 ± 0.006	15.625 ± 0.005
100	23.293 ± 0.007	21.234 ± 0.006	17.973 ± 0.005
250	22.481 ± 0.007	20.058 ± 0.006	17.289 ± 0.005
500	22.608 ± 0.007	19.167 ± 0.006	17.596 ± 0.005

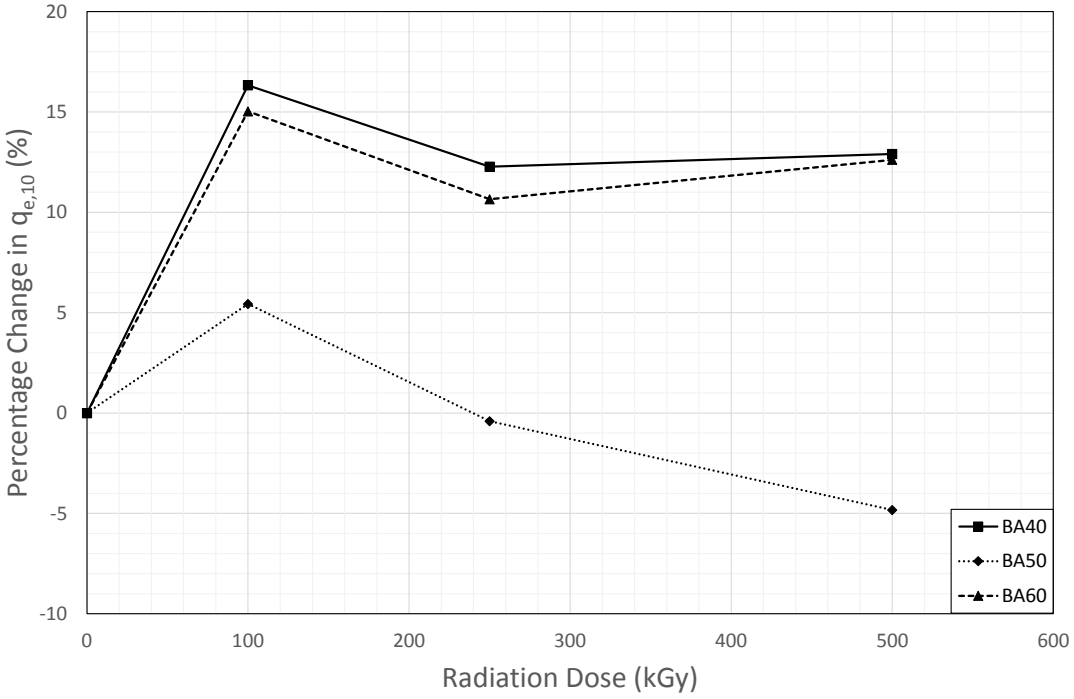

FIGURE 10: Percentage Change in $q_{e,10}$ Following Exposure to 100, 250 and 500 kGy Gamma Radiation under Standard Atmospheric Conditions.

DISCUSSION

Infra-red Spectroscopy

The small change in IR spectra seen, a maximum of 10%, is in agreement with the literature [12,17,26-27]. In BA40 the similar decreasing trend seen in the >C=C< *cis* and $R_1HC=CH_2$ vinylidene suggest the interaction of these two functional groups following BDN monomer ionisation. However, at higher doses the *trans* configuration of >C=C< and the C≡N nitrile begin to decrease, suggesting a crossover point at which the ACN unit begins to degrade through interaction with the *trans* vinyl functional groups on the BDN unit.

The spectra for BA50 showed more complex behaviour with degradation of the >C=C< *cis* and $R_1HC=CH_2$ vinylidene up to 10 kGy followed by the >C=C< *trans* up to 50 kGy, after which degradation of the *cis* and chain end groups resumed. However, the C≡N nitrile appeared to degrade at higher radiation doses as well. With the general decrease in peak height being lower than that seen in BA40 it is possible that in BA50 both the BDN and ACN units were becoming ionised simultaneously during radiation exposure.

In BA60 all backbone-attributable peak heights increased suggesting leaching of a substance that previously hindered the visibility of bond vibrations.

Material Properties

The steady increase seen in T_g suggested a general increase in gel content within all samples. This could also be interpreted as increasing cross link density and would explain the observed increase in RF and decreasing trend seen in the deviation of the relaxation curve on the stress-strain graph from the origin, Figure 11.

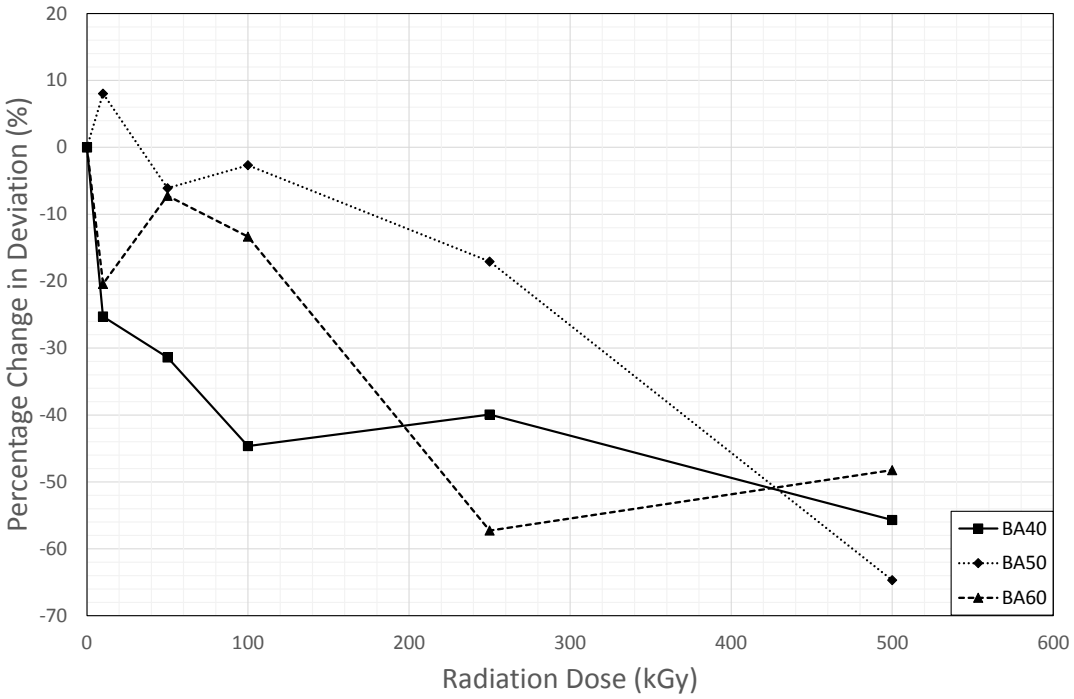

FIGURE 11: Percentage Change in Deviation from Origin for All Three Samples Following Exposure to 10, 50, 100, 250 and 500 kGy Gamma Radiation under Standard Atmospheric Conditions.

Absorption Behaviour

Toluene

The decrease in $\Delta_{M\%}$ with radiation dose for all samples is in agreement with *Hassan et al.* [27] and is due to the radiation-induced crosslinking resulting in a denser network of polymer chains.

CO_2

Kinetics

To assess the change in the k_2 vs C_e plots the integral of each data set was calculated between 3 and 17 g L^{-1} and its percentage change plotted against

radiation dose, Figure 12. All samples showed a decreasing trend suggesting a reduction in rate of uptake at higher radiation doses.

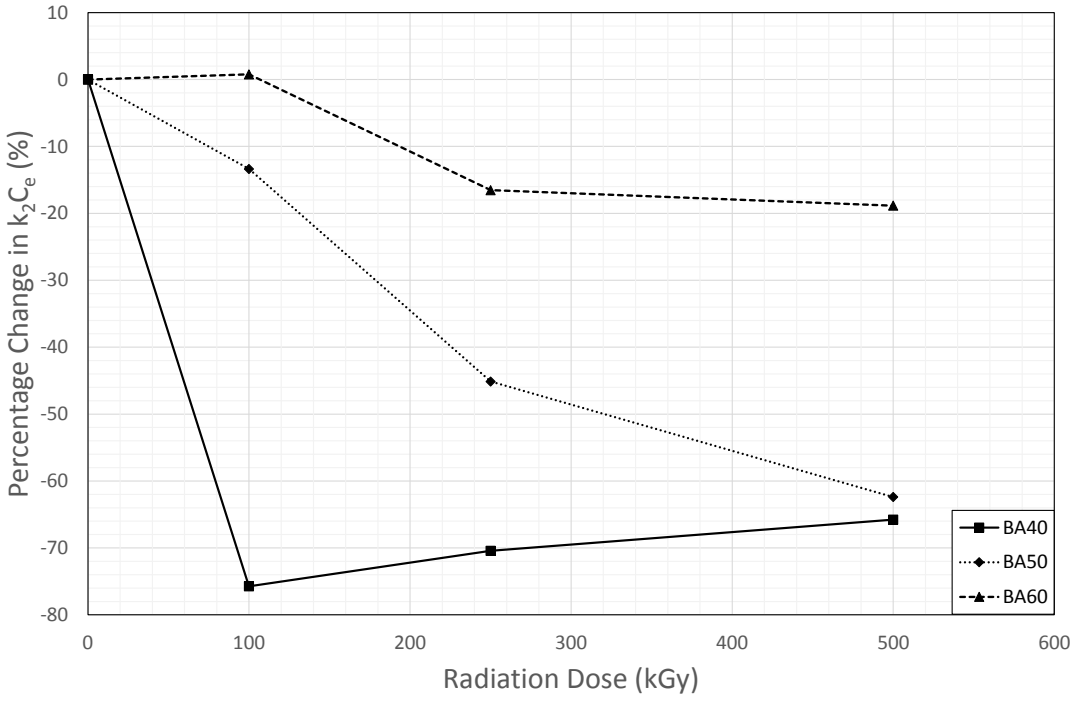

FIGURE 12: Percentage Change in k2.Ce Following Exposure to 10, 50, 100, 250 and 500 kGy Gamma Radiation under Standard Atmospheric Conditions.

Thermodynamics

It can be seen that the ultimate uptake did not change to the same degree as the kinetics and in fact saw an initial increase in total uptake for all samples. Following the fitting of the thermodynamic data to the Freundlich Isotherm, all samples exhibited an increase in both a_F and n_F following exposure to gamma radiation, Table 5. The largest change was seen in BA60 whilst BA50 appeared to initially increase and then decrease in both a_F and n_F, Figure 13.

TABLE 5: a_F and n_F for All Three Samples Following Exposure to 100, 250 and 500 kGy Gamma Radiation under Standard Atmospheric Conditions.

a_F			
Radiation Dose (kGy)	BA40	BA50	BA60
0	1.00±0.04	1.25±0.04	0.85±0.04
100	1.32±0.05	1.84±0.06	1.80±0.06
250	1.27±0.04	1.47±0.05	1.41±0.05
500	1.33±0.05	1.26±0.04	1.70±0.06
n_F			
Radiation Dose (kGy)	BA40	BA50	BA60
0	0.94±0.02	1.02±0.02	0.97±0.02
100	0.99±0.02	1.17±0.02	1.24±0.02
250	0.99±0.02	1.09±0.02	1.14±0.02
500	1.00±0.02	1.05±0.02	1.22±0.02

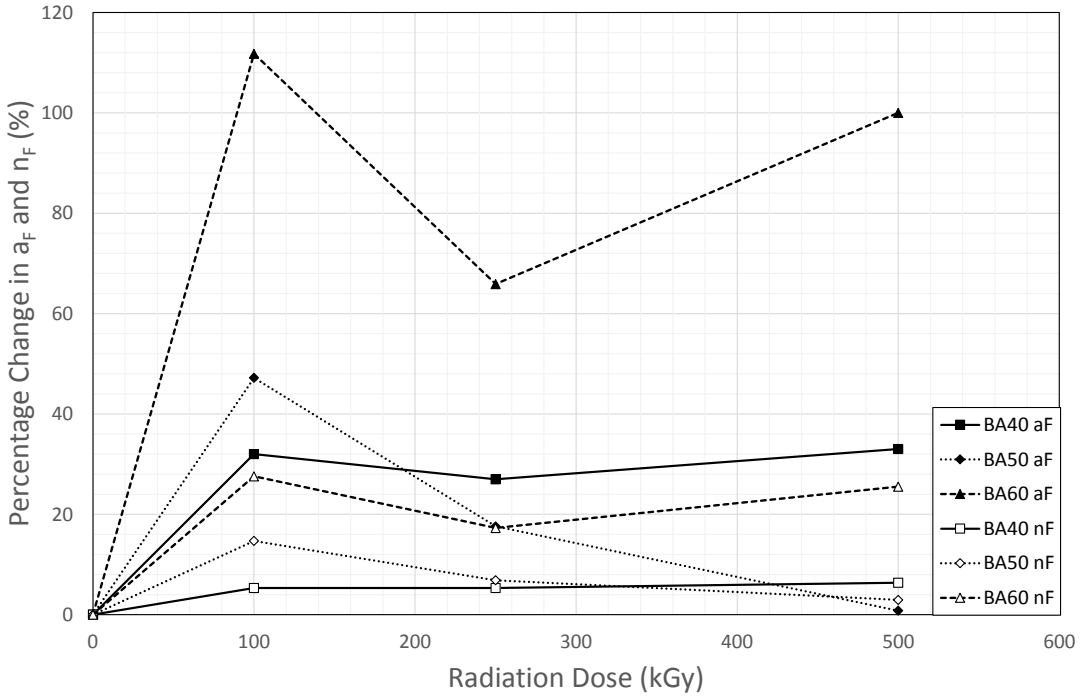

FIGURE 13: Percentage Change in a_F and n_F for All Three Samples Following Exposure to 100, 250 and 500 kGy Gamma Radiation under Standard Atmospheric Conditions.

The limited change seen in n_F suggested only a relatively small increase in the interaction between the polymeric structure and the CO_2 molecules whilst the larger increase in a_F suggested an overall increase in absorption potential of the samples. The greatest effect of this was seen in the harder samples.

Cross-comparison

Following the initial decrease in T_g seen in BA50 and BA60, all three commercial samples increased at a similar rate suggesting that the gamma-induced crosslinking is having the same effect on the gel content within all samples.

BA40 showed an almost immediate drop in k_2C_e followed by a steady increase. Both BA50 and BA60 showed a steadily decreasing trend with BA50 exhibiting the greatest change. When comparing to the IR spectra seen above, a trend is observed between the height of the BDN-representative peaks and the kinetics of CO_2 absorption. This suggests that the decrease in rate of uptake is due to a reduced affinity to the non-polar CO_2, a result of BDN degradation increasing the polarity of the elastomeric matrix.

Following irradiation the change in T_g for each sample was similar whilst there was a larger change seen in the harder materials for RF. This suggests that, following exposure to gamma radiation, the gel network increased at the same rate in each sample whilst the crosslink density increased at a higher rate in the harder samples. One explanation for this behaviour is the interaction between the elastomer chains and the larger proportion of fillers resulting in an increased number of chains becoming part of the gel network. Therefore the chains involved in the new crosslinks were already part of the gel network and therefore did not increase its value.

Vijayabaskar, Tikku and Bhowmick [12] exposed NBR samples to electron beam radiation and found that all characteristic properties, except for T_g, exhibited a larger change in the higher BDN containing samples. NMR analysis also revealed an increase in spectroscopic crosslink densities for samples with larger C-C linkages i.e. the higher BDN-containing samples. The propensity for the crosslink density of NBR samples to be affected by radiation is therefore proportional to their BDN content. However, for T_g and the portion of chains included in the gel network, it is the sample's ACN content that determines the degree of change induced by radiation. This can be explained by higher BDN contents instilling a greater proclivity for crosslink clustering.

The apparent decreased effect gamma radiation has on BA50 would suggest this sample to be the most resistant to radiation degradation. However, crosslink clustering would eventually lead to sample failure and with the reduced observable effects this degradation may be hidden and occur quite suddenly. As this ultimate failure was not reached in these tests and the total absorbed dose seen on site is far below those used here then the formation of crosslinks would only increase the capacity of this material to perform as a seal.

CONCLUSIONS

This report has investigated the effects of gamma radiation on glass transition temperature, mechanical response to compression, swelling capacity in toluene and CO_2 absorption behaviour and correlated the results against IR spectra to determine microstructural changes in the material that may affect its capacity to perform as a seal.

From the IR spectra it was suggested that BA40 initially degraded through ionisation of the BDN monomers which caused crosslinking between the *cis* C=C

in BDN and the $C=CH_2$ vinylidene groups. However, at higher radiation doses this was believed to shift towards a breakdown of the ACN monomers through an interaction between the *trans* C=C in BDN and the C≡N in ACN. BA50 appeared to degrade both monomers simultaneously.

The decrease of $\Delta_{M\%}$ and increase in T_g, required load for a set deflection and RF with radiation dose suggested the formation of crosslinks, which only began to hinder absorption in the latter phase of expansion, when a PSO model describes the rate of uptake. However, they have been shown to affect the affinity of the samples more than they affect the expansion of the network.

A comparison between the samples suggests an interaction between the strengthening filler particles and the polymer chains that negatively affects the rate of gel formation within the microstructure. A trend has been identified between BDN content and the potential for crosslink clustering that will reduce the dose effect and potentially increase radiation resistance in terms of physical and mechanical properties.

ACKNOWLEDGEMENTS

The authors would like to thank EDF Energy for the financial support that permitted this work and the technical assistance offered by Ruth Edge and Kevin Warren of the Dalton Cumbrian Facility.

REFERENCES

1. Datta, S.; Synthetic Elastomers in Rubber Technologists Handbook; White, J. R. and De, A. K., Eds.; iSmithers Rapra Publishing, 2001, pp. 47-74.
2. Achimsky, L., Audouin, L., Verdu, J., Rychly, J. and Matisova-Rychla, L. Polym. Degrad. Stabil., 1997, 58(3), 283-289.

3. Gillen, K. T., Celina, M. and Bernstein, R., Polym. Degrad. Stabil., 2003, 82(1), 25-35.
4. Howard, J. B. and Gilroy, H. M., Polym. Eng. Sci., 1975, 15(4), 268-271.
5. Kramer, E. and Koppelmann, J., Polym. Degrad. Stabil., 1986, 16(3), 261-275.
6. Oswald, H. J. and Turi, E., Polym. Eng. Sci., 1965, 5(3), 152-158.
7. Richters, P., Macromolecules, 1970, 3(2), 262-264.
8. Tamblyn, J. W. and Newland, G. C., J. Appl. Polym. Sci., 1965, 9(6), 2251-2260.
9. Celina, M., Gillen, K. T. and Assink, R. A., Polym. Degrad. Stabil., 2005, 90(3), 395-404.
10. Langlois, V., Audouin, L. and Verdu, J., Polym. Degrad. Stabil., 1993, 40(3), 399-409.
11. Davenas, J., Stevenson, I., Celette, N., Cambon, S., Gardette, J. L., Rivaton, A. and Vignoud, L., Nucl. Instrum. Meth. B., 2002, 191(1-4), 653-661.
12. Vijayabaskar, V., Tikku, V. K. and Bhowmick, A. K., Rad. Phys. Chem., 2006, 75, 779-792.
13. Hassan, M. M., Aly, R. O., El-Ghandour, A. H. and Abdelnaby, H. A., Elastom. Plast., 2013, 45(1), 77-94.
14. Cardona, F., Hill, D. J. T., Pomery, P. J. and Whittaker, A. K., Polym. Int., 1999, 48(10), 985-992.
15. Partridge, R. H., J. Chem. Phys., 1970, 52(5), 2501-2510.
16. Ahmed, F. S., Shafy, M., Abd El-megeed, A. A. and Hegazi, E. M., Mater. Des., 2012, 36, 823-828.

17. Hill, D. J. T., O'Donnell, J. H., Perera, M. C. S. and Pomery, P. J., J. Polm. Sci. Part A: Polym. Chem., 1996, 34(12), 2439-2454.
18. Porter, C. P. (2016), The safety and commercial implications of polymer seal degradation in a nuclear power generation application. PhD thesis, University of Sheffield.
19. Gosar, A. and Nagode, M., Int. J. Fatigue., 2012, 43, 160-167.
20. Ho, Y. S. and McKay, G., Proc. Saf. Environ. Prot., 1998, 76(4), 332-340
21. Freundlich, H. M. F., J. Phys. Chem., 1906, 57, 385-470.
22. Langmuir, I., J. Am. Chem. Soc., 1916, 38(11), 2221-2295.
23. Aharoni, C. and Ungarish, M., J. Chem. Soc., 1977, 73, 456-464.
24. Dubinin, M.M., Chem. Rev., 1960, 60(2), 235-241.
25. Ho, Y. S., Porter, J. F. and McKay, G., Water Air Soil Poll., 2002, 141(1), 1-33.
26. Zhao, W., Yu. L., Zhong, X., Zhang, Y. and Sun. J., J. Appl. Polym. Sci., 1994, 54(9), 1199-1205.
27. Hassan, M. M., Aly, R. O., El-Ghandour, A. H. and Abdelnaby, H. A., Elastom. Plast., 2013, 45(1), 77-94.